Linear and nonlinear photophysics and bioimaging of an integrin-targeting water-soluble fluorenyl probe†

Alma R. Morales,[a] Gheorghe Luchita,[a] Ciceron O. Yanez,[a] Mykhailo V. Bondar,[b] Olga V. Przhonska[b] and Kevin D. Belfield*[a,c]

Received 9th December 2009, Accepted 23rd March 2010
First published as an Advance Article on the web 8th April 2010
DOI: 10.1039/b925934a

Linear photophysical characterization and two-photon absorption (2PA) properties of a new water-soluble fluorene derivative, 3-(9-(2-(2-methoxyethoxy)ethyl)-2,7-bis{3-[2-(polyethyleneglycol-550-monomethylether-1-yl)]-4-(benzo[d]thiazol-2-yl)styryl}-9*H*-fluoren-9-yl)propanoic acid (**1**), were investigated in several organic solvents and water at room temperature. A comprehensive analysis of the steady-state absorption, emission and excitation anisotropy spectra revealed electronic structures of **1**, including mutual orientation of the transition dipoles, relatively weak solvatochromic effects, high fluorescence quantum yield (~0.5–1.0), and strong aggregation in water. The 2PA spectra of **1** were obtained in the 600–900 nm spectral range by two-photon induced fluorescence (2PF) and open aperture *Z*-scan methods using femtosecond laser sources. No discrete 2PA bands were apparent and values of the corresponding 2PA cross sections monotonically increased in the short wavelength range up to 3000 GM in organic solvents and ~6000 GM in aqueous solution, reflecting relatively high two-photon absorptivity. The 2PA efficiency of **1** in water increased 2–3 times relative to aprotic solvents and can be explained by cooperative electronic effects of molecular aggregates of **1** produced in aqueous media. The carboxylic acid fluorenyl probe **1** was conjugated with the cyclic peptide RGDfK. Two-photon fluorescence microscopy (2PFM) imaging of U87MG cells (and MCF-7 as control), incubated with fluorene-RGD peptide conjugate **2**, demonstrated high $\alpha_v\beta_3$ integrin selectivity, making this probe particularly attractive for integrin imaging.

Introduction

The synthesis and characterization of new molecules with high fluorescence quantum yield and efficient two-photon absorption (2PA) has been a subject of intense interest for numerous scientific and practical applications, such as two-photon fluorescence microscopy,[1–4] fluorescence-based sensing methodologies,[5–7] two-photon-induced lasing,[8,9] and 3D optical data storage.[10–12] Multiphoton fluorescence microscopy is a powerful tool for biological imaging and for the study of dynamic processes in living cells.[13–15] This application is dependent on the development of highly fluorescent, water-soluble, photochemically stable, multiphoton absorbing chromophores.[16,17] Most known fluorescent probes that can be utilized in one-photon fluorescence bioimaging are not optimized for two-photon excitation, and, as a rule, are characterized by relatively small 2PA cross sections δ_{2PA} ~ 10–100 GM[18,19] and corresponding action cross sections $\delta_{2PA}{}^{act} = \delta_{2PA} \cdot \eta$,[20] where η is the fluorescence quantum yield. The synthesis and characterization of water-soluble 2PA organic compounds for application in two-photon bioimaging has been reported.[16,21–24] The development of new water-soluble chromophores with biphenyl and dialkylfluorenyl core and three dodecyloxy end donor groups was described in ref. 16. These compounds exhibited 2PA cross sections up to 400 GM in the 500–550 nm range and modest values of δ_{2PA} in the near IR (~100 GM at 720 nm). Efficient 2PA of [2.2]paracyclophane-based fluorophores with high fluorescence quantum yield (~0.5–0.9) and corresponding cross sections of ~2000 GM in the presence of sodium dodecyl sulfate micelles was reported in ref. 22. The interaction of 2PA chromophores with micelles caused a large increase in the δ_{2PA} and $\delta_{2PA}{}^{act}$, among the highest reported in aqueous media. Hence, there still exists tremendous need for water-soluble probes containing high fluorescence quantum yield and high 2PA with the ability for conjugation for cell-, organelle-, or protein-specific targeting.

In this paper, the synthesis, linear photophysical characterization and 2PA properties of a new fluorene derivative, 3-(9-(2-(2-methoxyethoxy)ethyl)-2,7-bis{3-[2-(polyethyleneglycol-550-monomethylether-1-yl)]-4-(benzo[d]thiazol-2-yl)-styryl}-9*H*-fluoren-9-yl)propanoic acid (**1**), is described in both aprotic organic solvents and water. Comprehensive spectral analysis of the linear and nonlinear optical properties of this new water-soluble fluorenyl derivative **1**, along with its high fluorescence quantum yield and photochemical stability, makes this an intriguing candidate for use as a fluorescence probe. Additionally, conjugation of carboxylic acid functionality in **1** with the cyclic peptide RGDfK is presented. The resulting RGDfK conjugate (**2**) exhibited high $\alpha_v\beta_3$ integrin selectivity in both conventional

[a]*Department of Chemistry, University of Central Florida, Orlando, FL 32816-2366, USA*
[b]*Institute of Physics, Prospect Nauki, 46, Kiev-28, 03028, Ukraine*
[c]*CREOL, The College of Optics and Photonics, University of Central Florida, Orlando, FL 32816-2366, USA. E-mail: belfield@mail.ucf.edu; Fax: 4078232252; Tel: 4078231028*

† Electronic supplementary information (ESI) available: ^{1}H and ^{13}C NMR spectra are included for compounds **A**, **C**, **D**, **1**, and **2**. See DOI: 10.1039/b925934a

(one-photon) and two-photon fluorescence microscopy imaging, demonstrating the potential of this probe for integrin imaging.

Results and discussion

Synthesis

To induce increased solubility of fluorene derivatives in water, oligo(ethylene glycol) moieties were substituted on the phenyl ring of the styryl moiety. Poly- and oligo-(ethylene glycols) (PEG and OEG) have frequently been employed to prepare water-soluble polymers and therapeutic agents.[25] We prepared a new fluorescence probe of the A-π–π-π-A type, where A represents an electron-withdrawing moiety while π is a conjugated π-electron system, bearing long side chains averaging fifteen oxyethylene repeat units on the styryl phenyl ring (Scheme 1). The key step for the synthesis of the fluorenyl probe was a Pd-catalyzed Heck coupling reaction between oligo(2-methoxyethoxy)-4-vinylphenyl)benzo[d]thiazole (**D**) and 3-(9-(2-(2-methoxyethoxy)ethyl)-2,7-dibromo-9*H*-fluoren-9-yl)propanoic acid (**E**) (Scheme 1). The 2-(4-bromophenyl)benzo[d]thiazole (**B**) derivative was prepared by condensation of commercially available 2-aminobenzenethiol and 4-bromo-2-hydroxybenzoic acid in the presence of PPSE in *o*-dichlorobenzene, providing **B** as previously described.[26] Poly(ethylene glycol) monomethyl ether tosylate, $CH_3(OCH_2CH_2)n$OTs, was prepared by tosylation of the poly(ethyleneglycol)monomethylether at the alcohol terminus with tosyl chloride,[27] providing derivative **A** in 97% yield. Etherification was performed by refluxing tosylate **A** and 2-(4-bromophenyl)benzo[d]thiazole (**B**), together with K_2CO_3 in DMF at reflux. The oligo(2-methoxyethoxy)-4-bromophenyl)benzo[d]thiazole derivative was purified by column chromatography, and obtained in 85% yield (Scheme 1). Pd-catalyzed Stille coupling was subsequently performed between derivative **C** and tributyl(vinyl)tin in refluxing THF in a high pressure Schlenk tube with Pd(dppf)Cl_2·CH_2Cl_2 and CuI. After column chromatography, precursor **D** was obtained in 70% isolated yield. Pd-catalyzed Heck coupling reaction between 3-(9-(2-(2-methoxyethoxy)ethyl)-2,7-dibromo-9*H*-fluoren-9-yl)propanoic acid (**E**) and oligo(2-methoxyethoxy)-4-vinylphenyl)benzo[d]thiazole (**D**) was conducted in a high pressure Schlenk tube with $Pd(OAc)_2$, tri-*o*-tolylphosphine, and Et_3N as base in DMF at 90 °C, providing **1** in 70% yield (Scheme 1). EDC-mediated coupling between carboxylic acid **1** and cyclic RGDfK was carried out in the presence of sulfo-NHS in water at room temperature, affording the fluorene-RGD peptide conjugate **2** in 80% yield as shown in Scheme 2.

Linear spectral properties

The steady-state absorption, fluorescence, and excitation anisotropy spectra, and the primary photophysical parameters of probe **1** are presented in Fig. 1 and Table 1, respectively. The shape of absorption spectra and maximum values of extinction coefficients, ε^{max}, were concentration-independent in aprotic solvents up to $C \approx 2 \times 10^{-3}$ M. This indicates a negligible amount of aggregated molecules in aprotic media. In contrast, the shape of the absorption spectra in water exhibited a strong dependence on molecular concentration (Fig. 1b, curves 1, 2), which can be explained by molecular aggregation of **1** in polar protic solvent. The absorption band of the aggregates was not very sharp nor intense, as typically observed for large aggregated clusters.[28,29] In order to understand the nature of this aggregation, the dependencies of scattered light intensity, I, on excitation wavelength, λ, were obtained in the spectral range of one-photon transparency, $\lambda \geq 720$ nm, in protic and aprotic media, and presented in Fig. 2. As can be deduced from Fig. 2, the dependencies $I = f(1/\lambda^4)$ are close to a linear function for all the investigated solutions, strongly suggestive of a Rayleigh-type scattering mechanism.[30] Taking into

Table 1 Main photophysical parameters of **1** in solvents with different polarity Δf: absorption λ_{abs}^{max} and fluorescence λ_{fl}^{max} maxima, Stokes shifts, maximum extinction coefficients, ε^{max}, fluorescence lifetimes, τ, and quantum yields, Φ

N/N	Chloroform	ACN	Water[a]
Δf	0.149	0.305	0.32
λ_{abs}^{max}/nm	412 ± 1	409 ± 1	432 ± 1
λ_{fl}^{max}/nm	452 ± 1	479 ± 1	509 ± 1
Stokes shift/nm	40 ± 2	70 ± 2	77 ± 2
$\varepsilon^{max}/10^{-3}$ M^{-1} cm^{-1}	115 ± 10	125 ± 10	107 ± 10
Φ	1 ± 0.05	1 ± 0.05	0.5 ± 0.03
τ/ns	0.80 ± 0.04	0.98 ± 0.04	1.21 ± 0.05 0.4 ± 0.1

[a] Concentration of **1** in water $C \approx 10^{-6}$ M.

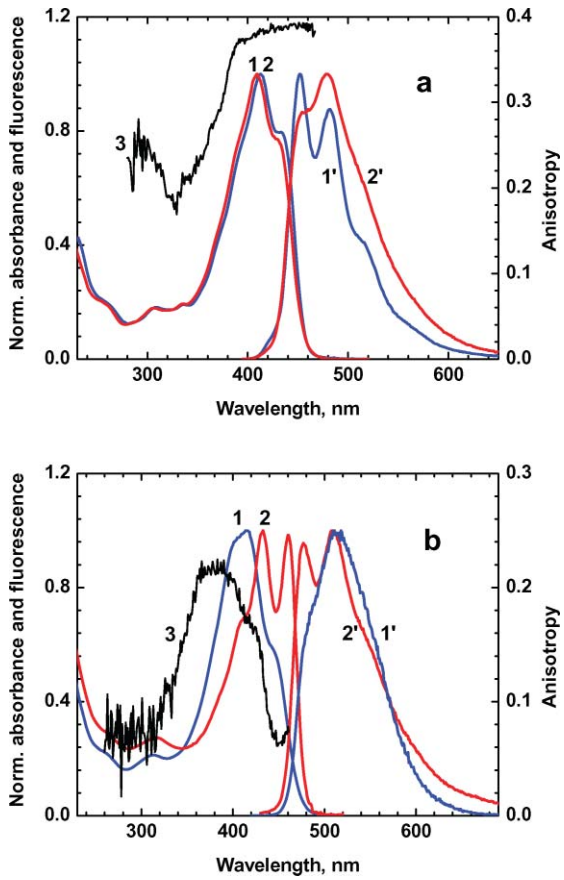

Fig. 1 Normalized absorption (1, 2), fluorescence (1′, 2′) and excitation anisotropy (3) spectra of **1** in: (a) chloroform (1, 1′), ACN (2, 2′) and poly-THF (pTHF) (3); (b) water with chromophore concentration $C \approx 10^{-3}$ M (1, 1′), $C \approx 10^{-6}$ M (2, 2′) and glycerol with $C \approx 10^{-6}$ M (3).

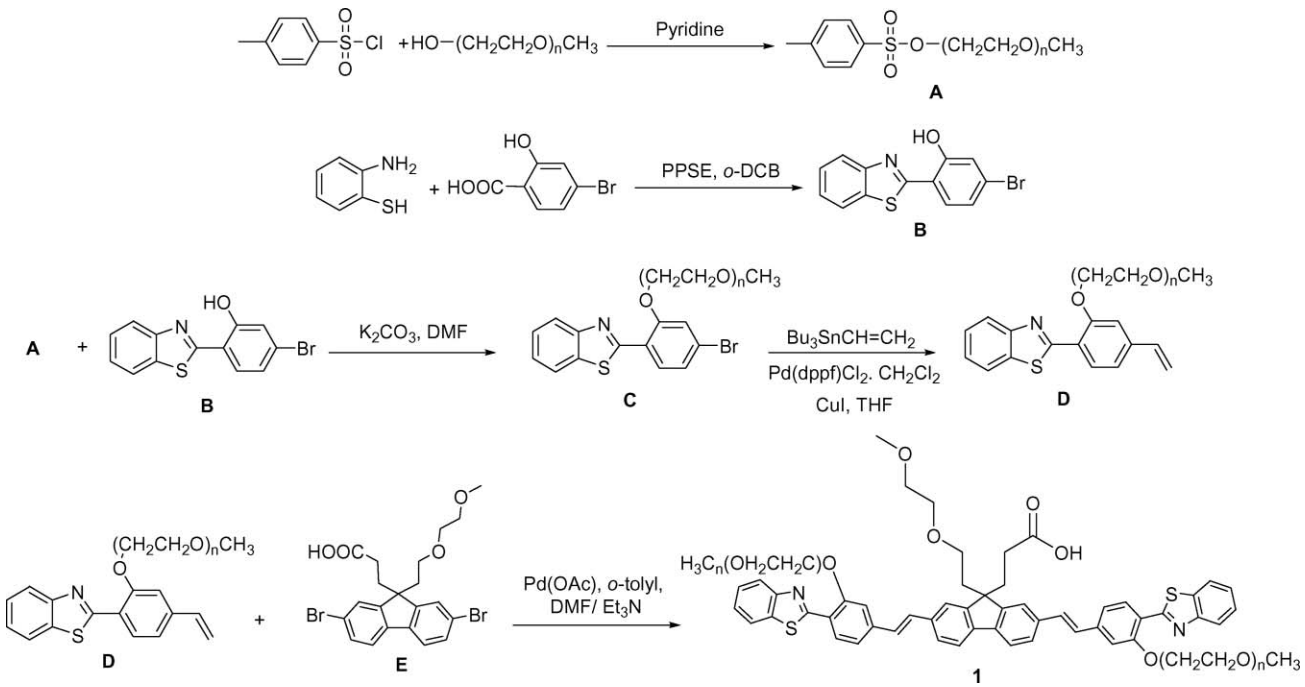

Scheme 1 Synthesis of water-soluble fluorescent probe **1**.

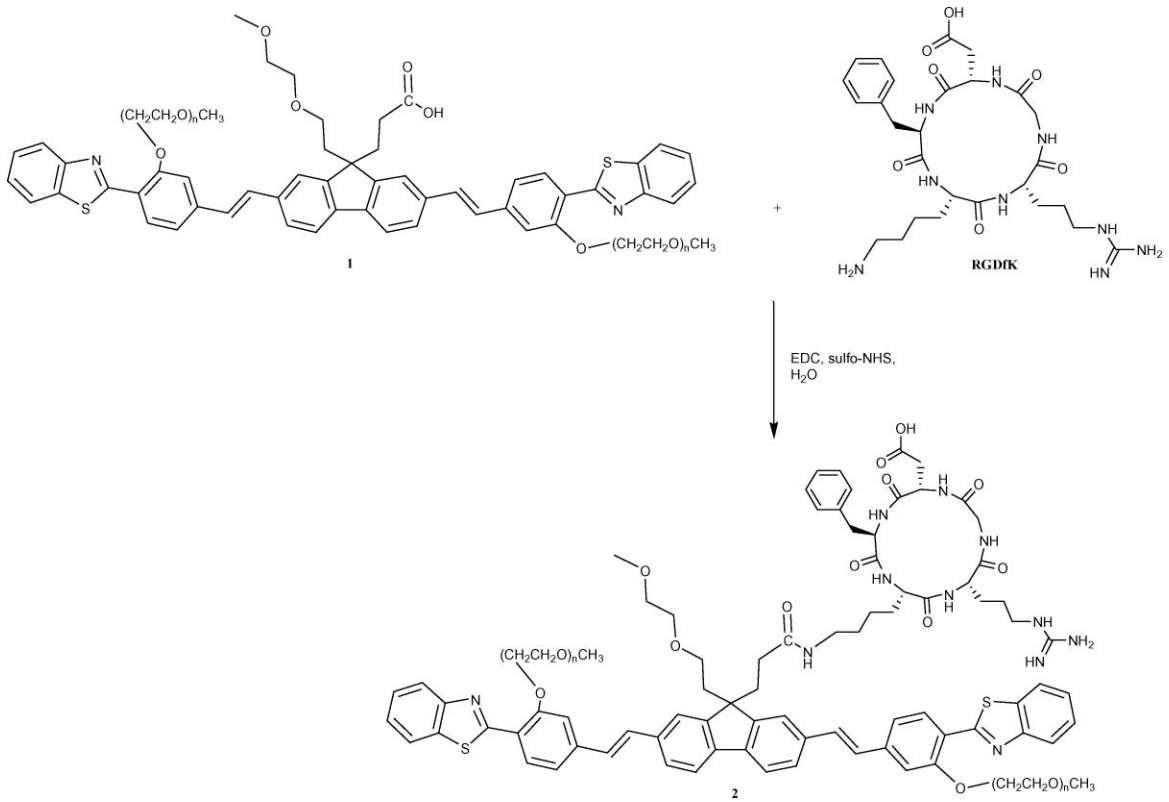

Scheme 2 Synthesis of fluorene-RGDfK peptide conjugate **2**.

account, that, for Rayleigh scattering, $I \sim I_0 r^6/\lambda^4$ (r is the size of scattering centers), we can estimate the difference in the size r for aggregated and monomer molecules from the data in Fig. 2, which were obtained under the same experimental conditions. Analysis of this data revealed dimers as the most probable aggregates of **1** in water. This is consistent with the relatively broad absorption spectrum of these aggregates (Fig. 1b, curve 1).

The absorption spectra of **1** in aprotic solvents were nearly independent of solvent polarity, Δf (Fig. 1a, curves 1, 2), and exhibited a well-defined vibrational structure in low concentration

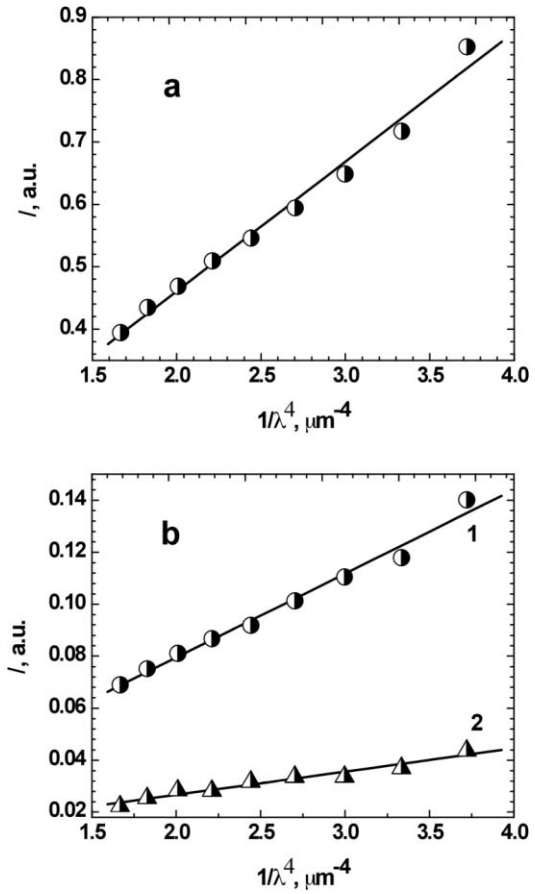

Fig. 2 Dependences $I = f(1/\lambda^4)$ for **1** in: (a) water; (b) ACN (1) and chloroform (2).

aqueous solution (Fig. 1b, curve 2). The fluorescence spectra of **1** are characterized by a weak solvatochromic effect with increased Stokes shift up to ~80 nm in water. It is interesting to note that in high concentrations in aqueous solution, the formation of molecular dimers of **1** exhibited an increased Stokes shift (~100 nm) with no apparent vibrational structure (Fig. 1b, curves 1, 1′). In this case, the fluorescence spectrum is similar to the charge transfer emission band.[31] It should be mentioned that fluorescence spectra were independent of excitation wavelength in aprotic solvents and exhibited this dependence only in protic media (water, glycerol).

The excitation anisotropy spectrum of **1** in viscous pTHF (Fig. 1a, curve 3) provided information on the nature of the one-photon absorption band in aprotic media. Nearly constant values of $r_0 \approx 0.38$ in the 400–450 nm spectral range is close to the theoretical limit (0.4),[31] and primarily corresponds to a single electronic transition, S_0–S_1. This means that there is nearly parallel orientation ($\alpha \leq 10°$, see eqn (1) in the Experimental section) of the absorption $S_0 \rightarrow S_1$ and emission $S_1 \rightarrow S_0$ transition dipoles of **1**, allowing one to estimate the angles between $S_0 \rightarrow S_1$ and $S_0 \rightarrow S_n$ absorption transitions ($n = 2, 3, \ldots$). From Fig. 1a (curve 3), the values of $r_0 \geq 0.2$ in the spectral range $\lambda < 400$ nm corresponded to $\alpha \leq 35°$. The decay of fluorescence emission of **1** in chloroform and ACN (polar aprotic solvents) was characterized by a single exponential process with typical lifetimes $\tau \approx 0.8$–1 ns (see Table 1) and high fluorescence quantum yield $\Phi \approx 1.0$.

In contrast to these aprotic solvents, the value of r_0 in glycerol (Fig. 1b, curve 3) was not constant in the main absorption band, indicative of the rather complex electronic nature of **1** in polar protic media. This nature can be attributed to specific solute–solvent effects such as hydrogen bonding[32] and inhomogeneous broadening of the solvated molecules.[33] Fluorescence decay of **1** in protic polar media corresponded to a double exponential process with short (~0.4 ns) and long (~1.2 ns) components and decreased fluorescence quantum yield (see Table 1). The pre-exponential coefficients were $A_1 = 0.88$ and $A_2 = 0.12$ for the short ($t_1 = 0.4$ ns) and long ($t_2 = 1.21$ ns) lifetime components, respectively, suggesting predominant aggregate formation in water. This provides further evidence of specific solvent effects and is consistent with the excitation anisotropy spectra.

2PA properties of 1

The efficiency of 2PA processes for **1** was investigated in aprotic solvents and water at room temperature. The corresponding spectra are presented in Fig. 3. No discrete 2PA peaks were observed in the main one-photon absorption (1PA) band, $\lambda \approx 350$–450 nm, and the values of two-photon cross sections δ_{2PA} increased monotonically in the short wavelength spectral range, and were independent of solvent polarity in aprotic media. The molecular structure of **1** is unsymmetrical (C_1 point group symmetry), but the π-conjugated system of this chromophore possesses nearly symmetrical electronic distribution. Alkyl groups in the 9-position and oxygen-containing substituents in **1** do not strongly affect the π-electronic distribution. Therefore, the efficiency of the two-photon transition $S_0 \rightarrow S_1$ is noticeably suppressed by dipole selection rules[34] and no 2PA maximum was detected in this spectral region. This behavior is typical for symmetrical (C_{2v}) fluorene derivatives (see ref. 35). Nevertheless, the absolute values of the 2PA cross sections reach $\delta_{2PA} \sim 100$–1000 GM at $\lambda \approx 690$–800 nm, values that are quite suitable for two-photon bioimaging using commercially available femtosecond lasers. The extreme points at $\lambda \approx 300$–310 nm in the excitation anisotropy spectra of **1** in aprotic solvents and water (see Fig. 1, curves 3) indicates weak one-photon electronic transitions that are slightly resolved in the 1PA spectra (curves 1, 2). These transitions can be effective in the 2PA processes

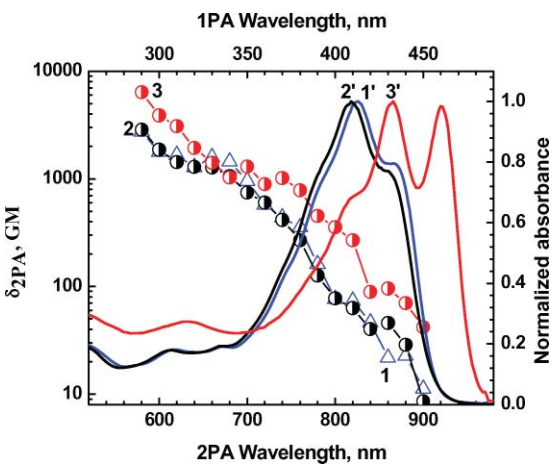

Fig. 3 2PA spectra of **1** in chloroform (1), ACN (2) and water (3). Normalized linear absorption (1PA) of **1** in chloroform (1′), ACN (2′) and water (3′). Experimental errors of (1–3) ± 15%.

and used to determine the monotonic increase in δ_{2PA} in the short wavelength spectral range. On the other hand, the increase in δ_{2PA} is also induced by the change in the detuning energy, $E = hc(1/\lambda^{max}_{ab} - 1/\lambda)$, where c and h are the speed of light in vacuum and Planck's constant, respectively.[36] It should be mentioned that the differences observed in δ_{2PA} for **1** in aprotic solvents and water cannot be explained by the corresponding changes in the value of E only. A comprehensive analysis of the linear spectral data (Table 1) supports a significant role of aggregation processes in increasing the 2PA cross section of **1** in aqueous medium. According to Fig. 3, the value of δ_{2PA} increased 2–3 times in water relative to aprotic solvents, reaching 6000 GM at $\lambda \approx 600$ nm. Similar cooperative effects in 2PA were observed for PIC and porphyrin J-aggregates in aqueous solutions.[37,38]

Single and two-photon fluorescence cell imaging

To demonstrate the potential of this new dye in selective two-photon fluorescence bioimaging, a targeting vector was incorporated. To achieve target selectivity, the sequence Arg-Gly-Asp (RGD) was chosen as it is recognized by a number of integrins.[39] Integrins are a family of plasma membrane glycoproteins formed by several α and β subunits. These subunits are long molecular weight polypeptide chains that form a receptor when α–β heterodimers are formed. Of the 25 distinct pairs of heterodimers that have been reported, $\alpha_v\beta_3$ integrin has unique properties, in that it is known to bind to specific extracellular matrix molecules (fibronectin, fibrogen, and vibronectin). It is also upregulated in invasive tumor cells, yet not significantly expressed in quiescent endothelial cells nor in normal tissue,[40] making this integrin of particular interest when targeting angiogenic vasculature and tumor cells alike.[41]

In order to test the selectivity of fluorene-RGD peptide conjugate **2** *in vitro*, U87MG human gliobastoma cells were selected as a positive control due to its elevated $\alpha_v\beta_3$ integrin expression. Low $\alpha_v\beta_3$ integrin expressing MCF-7 human breast cancer cells served as a negative control.[41] Cells incubated for the same period of time at the same dye concentration showed significantly different results for the two different cell lines (positive and negative controls), as shown in Fig. 4 and 5, respectively. In the positive control images, specific staining of the cells was observed. Furthermore, enhanced image resolution for two-photon fluorescence microscopy (2PFM) *vs.* conventional or one-photon fluorescence microscopy imaging was clearly observed, both in terms of spatial resolution and in contrast (Fig. 4).

The specificity of fluorene-RGD probe **2** enabled the labeling and visualization of sites where higher concentrations of the integrin are localized within the cells. Integrins play an important role in cell adhesion to the extra cellular matrix, ECM, and in the signaling processes that depend on or regulate adhesion. This means that integrin is at the center of an array of cell processes such as cell migration, shape, survival, proliferation, and gene transcription.[40,42] Once integrins bind to their extracellular ligand, they cluster in focal spots that are rich in actin and actin-associated proteins. These spots, called *focal adhesions* (FA's) or *focal contacts*, can clearly be seen in cultured fibroblast, where the cell surface is separated from the substratum by 10 to 15 μm only at these localized regions (whereas in the rest of the cell the distance is approximately 50 μm).[43,44]

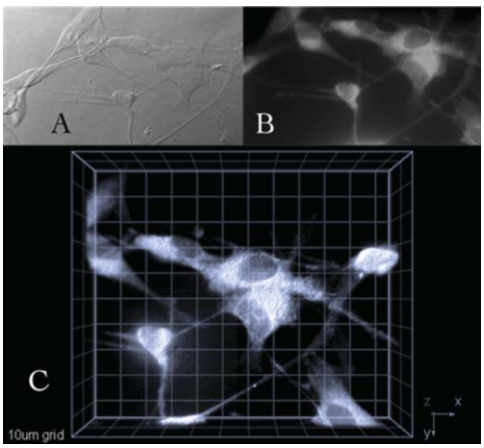

Fig. 4 One-and two-photon fluorescence micrographs of U87MG cells incubated with probe **2** (50 μM, 30 min). (A) DIC, (B) one-photon fluorescence, (C) 3D reconstruction from overlaid 2PFM images, 76 MHz, 115 fs pulse width, 700 nm, 60× objective (NA = 1.35, Olympus). Scale: 10 μm grid.

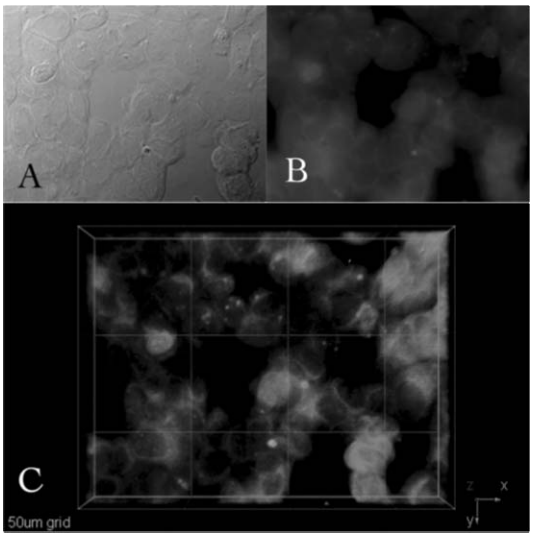

Fig. 5 One-and two-photon fluorescence micrographs of MCF-7 cells incubated with probe **2** (50 μM, 30 min). (A) DIC, (B) one-photon fluorescence, (C) 3D reconstruction from overlaid 2PFM images, 76 MHz, 115 fs pulse width, 700 nm, 60× objective (NA = 1.35, Olympus). Scale: 10 μm grid.

In the U87MG cells that were incubated with probe **2**, it was observed that a higher concentration of the probe **2** was present in areas that appear to be FA's (Fig. 6) in the motile zone (IV) and culling zone (III) of a polarized cell. In the magnification of the motile zone (Fig. 6B), these apparent FA's are visualized quite clearly by 2PFM. In the persistence zone of the cell (Fig. 6A, III), more FA's were observed and higher fluorescence in other localized spots can be attributed to the endoplasmic reticulum with newly synthesized or stored integrin. Furthermore, nascent focal adhesion points can be seen in the formation zone (I) of the cell, as indicated by the arrow in Fig. 6A. These micrographs show the selectivity that fluorenyl-RGD peptide **2** has for $\alpha_v\beta_3$ integrin, and the potential that this 2PA fluorescent probe has for studying integrin-mediated processes in cells or tissue *in vitro*, and, perhaps, *in vivo*.

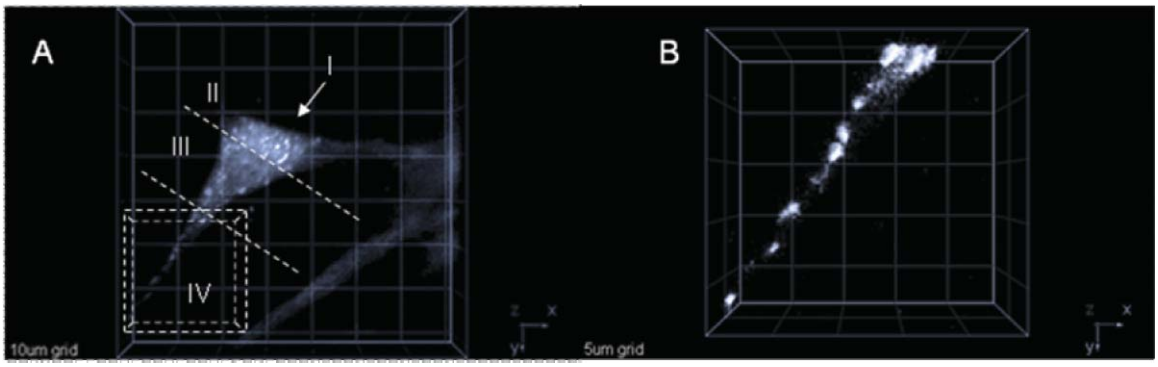

Fig. 6 (A) Two-photon fluorescence micrograph of U87MG cells incubated with probe **2** (50 μM, 30 min). 3D reconstruction from overlaid 2PFM images, 76 MHz, 115 fs pulse width, 700 nm, 60× objective (NA= 1.35, Olympus). (B) Magnification of volume indicated by cube in A. Scale: 10 μm grid in A and 5 μm in B.

Experimental

Materials and Synthetic Procedures

The synthesis of 2-(benzo[d]thiazol-2-yl)-5-bromophenol (**B**) and 3-(9-(2-(2-methoxyethoxy)ethyl)-2,7-dibromo-9*H*-fluoren-9-yl)propanoic acid (**E**) was described previously.[26,45] Pd-catalyzed reactions were performed in high pressure Schlenk tubes under N_2. All reagents and solvents were used as received from commercial suppliers, unless otherwise noted. ^{1}H and ^{13}C NMR spectroscopic measurements were performed using a Varian 500 NMR spectrometer at 500 or 125 MHz, respectively, with tetramethysilane (TMS) as internal reference; ^{1}H (referenced to TMS at δ = 0.0 ppm) and ^{13}C (referenced to $CDCl_3$ at $\delta = 77.0$ ppm). Chemical shifts of ^{1}H and ^{13}C spectra were interpreted with the support of CS ChemDraw Ultra version 5.0. High-resolution mass spectrometry (HR-MS) analysis was performed in the Department of Chemistry, University of Florida, Gainesville, FL.

Synthesis of $CH_3(OCH_2CH_2)_nOTs$ (A). Sodium hydroxide (2.18 g, 54.52 mmol) in water (12 mL), and poly(ethylene glycol) methylether $CH_3(OCH_2CH_2)_nOH$ (12 g, 21.81 mmol) in THF (12 mL) were cooled in an ice bath with stirring, and *p*-toluenesulfonyl chloride (5.03 g, 26.39 mmol) in THF (12 mL) was added dropwise over 1 h. The reaction mixture was stirred for additional 2 h at 5 °C, poured into ice water, and extracted with CH_2Cl_2 (200 mL). The combined organic extracts were washed with dilute HCl followed by brine (50 mL), then dried over $MgSO_4$, and the solvent removed *in vacuo* to yield **A** (12.6 g, 82% as colorless oil). ^{1}H NMR (500 MHz, $CDCl_3$) δ: 7.80 (d, J = 8 Hz, 2H), 7.36 (d, J = 8 Hz, 2H), 4.38 (bs, 6H), 4.16, (t, J = 5, 2H), 3.73-3.54 (bm, 45H), 3.39 (s, 3H), 2.45 (s, 3H). ^{13}C NMR (125 MHz) δ: 144.80, 132.81, 130.03, 129.58, 127.95, 127.83, 127.76, 71.78, 71.22, 70.97, 70.64, 70.58, 70.50, 70.39, 70.28, 70.16, 69.42, 69.25, 69.09, 68.99, 68.79, 68.55, 58.89, 21.67. HRMS-ESI: found $[C_7H_8O_3S(C_2H_4O)_{16}CH_3+Na]^+ = 913.43$, requires [M+Na, 913.44]$^+$; found $[C_7H_8O_3S(C_2H_4O)_{15}CH_3+Na]^+$ = 869.41, requires [M+Na, 871.42]$^+$; found $[C_7H_8O_3S(C_2H_4O)_{14}CH_3+Na]^+$ = 825.38, requires [M + Na, 825.39]$^+$; found $[C_7H_8O_3S(C_2H_4O)_{13}CH_3+Na]^+$ = 781.36, requires [M+Na, 781.37]$^+$; found $[C_7H_8O_3S(C_2H_4O)_{12}CH_3+Na]^+$ = 737.37, requires [M+Na, 737.34]$^+$; found $[C_7H_8O_3S(C_2H_4O)_{11}CH_3+Na]^+$ = 693.31, requires [M+Na, 693.31]$^+$; found $[C_7H_8O_3S(C_2H_4O)_{10}CH_3+Na]^+$ = 649.28, requires [M+Na, 649.29]$^+$; found $[C_7H_8O_3S(C_2H_4O)_9CH_3+Na]^+$ = 605.25, requires [M+Na, 605.26]$^+$; found $[C_7H_8O_3S(C_2H_4O)_8CH_3+Na]^+ = 561.23$, requires [M+Na, 561.23]$^+$; found $[C_7H_8O_3S(C_2H_4O)_7CH_3+Na]^+ = 517.20$, requires [M+Na, 517.21]$^+$; found $[C_7H_8O_3S(C_2H_4O)_6CH_3+Na]^+$ = 450.16, requires [M+Na, 450.19]$^+$; found $[C_7H_8O_3S(C_2H_4O)_5CH_3+Na]^+$ = 429.13, requires [M+Na, 429.16]$^+$; found $[C_7H_8O_3S(C_2H_4O)_4CH_3+H]^+ = 363.19$, requires [M+Na, 362.14]$^+$; found $[C_7H_8O_3S(C_2H_4O)_3CH_3+H]^+$ = 319.17, requires [M+H, 318.11]$^+$; found $[C_7H_8O_3S(C_2H_4O)_2CH_3+H]^+$ = 275.14, requires [M+H, 274.09]$^+$.

Synthesis of 2-[2-(polyethyleneglycol-550-monomethylether-1-yl)-4-bromophenyl]benzo[d]thiazole (C). A mixture of benzothiazol-2-yl-5-bromophenol (2.45 g, 7.95 mmol) and $CH_3(OCH_2CH_2)_nOTs$ (7.27 g, 10.33 mmol) was dissolved in 25 mL of DMF. To this, K_2CO_3 (23.85 g) was added and the solution was stirred at reflux for 4 h. After cooling to room temperature, the solution was filtered, poured into water, and extracted thrice with CH_2Cl_2. The combined organic layers were washed with water and then with brine, dried over magnesium sulfate, filtered, and the solvent was removed at reduced pressure. Chromatography (silica gel, ethyl acetate–MeOH 9 : 1) provided **C** (6.04 g, 85%) as colorless oil.^{1}H NMR (500 MHz, $CDCl_3$) δ: 8.42 (d, J = 8 Hz, 1H), 8.08 (d, J = 8.5 Hz, 1H), 7.93 (d, J = 7.5 Hz, 1H), 7.51 (t, J = 7 Hz, 1H), 7.39 (t, J = 7 Hz, 1H), 7.27 (t, J = 8.5 Hz, 1H), 4.38 (t, J = 10 Hz, 2H), 4.07 (t, J = 5.5 Hz, 2H), 3.80 (t, J = 5 Hz, 2H), 3.71-3.53 (m, 51H), 3.37 (s, 3H). ^{13}C NMR (125 MHz,δ $CDCl_3$) δ: 162.15, 156.74, 151.93, 151.91, 136.07, 136.05, 130.71, 130.45, 126.20, 125.87, 125.42, 124,97, 124.78, 124.58, 124.33, 122.84, 122.71, 121.54, 121.25, 116.36, 115.92, 71.89, 70.88, 70.74, 70.67, 70.64, 70.52, 70.41, 70.28, 69.53, 69.37, 69.20, 68.85, 59.04. HRMS-ESI: found $[C_{13}H_7BrNOS(C_2H_4O)_{15}CH_3+Na]^+$ = 1004.27, requires [M+Na, 1004.35]$^+$; found $[C_{13}H_7BrNOS(C_2H_4O)_{14}CH_3+Na]^+ = 960.30$, requires [M+Na, 960.32]$^+$; found $[C_{13}H_7BrNOS(C_2H_4O)_{13}CH_3+Na]^+$ = 916.29, requires [M+Na, 916.30]$^+$; found $[C_{13}H_7BrNOS(C_2H_4O)_{12}CH_3+Na]^+$ = 872.26, requires [M+Na, 872.27]$^+$; found $[C_{13}H_7BrNOS(C_2H_4O)_{11}CH_3+Na]^+$ = 828.23, requires [M+Na, 828.25]$^+$; found $[C_{13}H_7BrNOS(C_2H_4O)_{10}CH_3+Na]^+$ = 784.21, requires [M+Na, 784.22]$^+$; found $[C_{13}H_7BrNOS(C_2H_4O)_9CH_3+Na]^+$ = 740.19,

requires [M+Na, 740.19]$^+$; found [$C_{13}H_7BrNOS(C_2H_4O)_8CH_3$+Na]$^+$ = 696.16, requires [M+Na, 696.17]$^+$.

Synthesis of 2-[2-(polyethyleneglycol-550-monomethylether-1-yl)-4- vinylphenyl)benzo[d]thiazole (D). Compound **C** (3 g, 3.94 mmol), Pd(dppf)Cl_2·CH_2Cl_2 (0.32 g, 0.39 mmol), and CuI (0.15 g, 0.78 mmol) were transferred to a high pressure Schlenk tube, followed by addition of THF (50 mL) and tributyl(vinyl)tin (1.62 g, 5.12 mmol). The Schlenk tube was sealed and stirred at 90 °C. After 96 h, silica gel TLC indicated disappearance of the aryl bromide. Hence, the dark brown reaction mixture was cooled to room temperature, diluted CH_2Cl_2, and filtered through a plug of silica gel. The crude product was concentrated and purified by column chromatography on silica gel using ethyl acetate–MeOH (4 : 1) providing **D** (2.1 g, 71%) as colorless oil. ^{1}H NMR (500 MHz, $CDCl_3$) δ: 8.48 (d, J = 8.5 Hz, 1H), 8.06 (d, J = 6 Hz, 1H), 7.91 (d, J = 8 Hz, 1H), 7.48 (t, J = 15 Hz, 1H), 7.36 (t, J = 14.5 Hz,1H), 7.17 (d, J = 8 Hz, 1H), 7.07 (s, 1H), 6.74 (q, J = 17.5 Hz, 1H), 5.86 (d, J = 17.5 Hz, 1H), 5.36 (d, J = 10.5 Hz, 1H), 4.40 (t, J = 10 Hz, 2H), 4.07 (t, J = 10 Hz, 2H), 3.79 (t, J = 9 Hz, 2H), 3.69-3.51 (m, 59H), 3.35 (s, 3H).^{13}C NMR (125 MHz, $CDCl_3$) δ: 162.87, 156.62, 152.01, 141.04, 136.19, 136.10, 136.12, 129.71, 129.55, 126.0, 125.74, 124.66, 124.43, 122.66, 121.22, 119.44, 119.22, 110.38, 110.18, 71.88, 70.85, 70.65, 70.60, 70.48, 70.34, 69.69, 69.53, 69.35, 68.44, 59.01, 58.98. HRMS-ESI: found [$C_{15}H_{10}NOS(C_2H_4O)_{15}CH_3$+Na]$^+$ = 950.32, requires [M+Na, 950.41]$^+$; found [$C_{15}H_{10}NOS(C_2H_4O)_{14}CH_3$+Na]$^+$ = 906.38, requires [M+Na, 906.43]$^+$; found [$C_{15}H_{10}NOS(C_2H_4O)_{13}CH_3$+Na]$^+$ = 862.36, requires [M+Na, 862.4]$^+$; found [$C_{15}H_{10}NOS(C_2H_4O)_{12}CH_3$+Na]$^+$ = 818.37, [M+Na, 818.38]$^+$; found [$C_{15}H_{10}NOS(C_2H_4O)_{11}CH_3$+Na]$^+$ = 774.34, requires [M+Na, 774.35]$^+$; [$C_{15}H_{10}NOS(C_2H_4O)_{10}CH_3$+Na]$^+$ = 730.32, requires [M+Na, 730.32]$^+$; found [$C_{15}H_{10}NOS(C_2H_4O)_9CH_3$+Na]$^+$ = 686.29, requires [M+Na, 686.30]$^+$.

Synthesis of 3-(9-(2-(2-methoxyethoxy)ethyl)-2,7-bis{3-[2-(polyethyleneglycol-550-monomethylether-1-yl)]-4-(benzo[d]thiazol-2-yl)styryl}-9*H*-fluoren-9-yl)propanoic acid (1). 3-(9-(2-(2-Methoxyethoxy)ethyl)-2,7-dibromo-9*H*-fluoren-9-l)propanoic acid (**E**) (0.17 g, 0.34 mmol), benzothiazole derivative **D** (0.55 g, 0.78 mmol), $Pd(OAc)_2$ (0.03 g, 0.13 mmol), and P(*o*-tolyl)$_3$ (0.068 g, 0.22 mmol) were transferred to a high pressure Schlenk tube. To this 8 mL of DMF–Et_3N (5 : 1 v/v) was added. The Schlenk tube was then sealed and stirred at 90 °C for 72 h. The mixture was cooled to room temperature and filtered. The solvent was removed under reduced pressure. The crude product was purified by column chromatography on silica gel first using ethyl acetate, then ethyl acetate–MeOH (4 : 1) and MeOH as eluent to afford **1** (0.4 g, 82%) as yellow-brownish solid. ^{1}H NMR (500 MHz, *d*-DMSO) δ: 8.46 (d, J = 8 Hz, 2H), 8.12 (d, J = 8 Hz, 2H), 8.06 (d, J = 8 Hz, 2H), 7.86 (t, J = 15.5 Hz, 4H), 7.65-7.42 (m, 14H), 4.52 (s, 4H), 4.03 (bt, J = 8.5 Hz, 4H), 3.73 (t, J = 5.5 Hz 4H), 3.62 -3.10 (m, 125H), 2.71 (bt, 2H), 2.43 (bt, 4H), 2.24 (bt, 2H). ^{13}C NMR (125 MHz, *d*-DMSO) δ: 175.99, 162.58, 156.95, 152.11, 150.64, 141.88, 140.51, 136.62, 136.06, 131.61, 129.47, 129.26, 127.91, 127.34, 127.03, 126.73, 126.29, 125.04, 124.81, 122.83, 122.67, 122.19, 122.01, 121.64, 120.77, 120.11, 119.77, 111.53, 111.24, 110.86, 79.71, 79.45, 79.18, 71.89, 71.78, 71.57, 70.97, 70.78, 70.69, 70.46, 70.39, 70.28, 70.21, 70.02, 69.97, 69.77, 69.64, 69.52, 69.47, 69.41, 69.30, 68.89, 68.53, 68.29, 67.20, 59.10, 58.59, 58.36, 58.18, 57.86, 57.62, 52.56, 36.68, 31.08. HRMS-ESI: High resolution MS shows a series of ions centered around m/z 2246 [$C_{51}H_{40}N_2O_6S_2(C_2H_4O)_{32}C_2H_6 - CH_3O$]$^+$ which are fragments related to the various ethoxylate oligomers that differ by $\Delta m/z$ 44, an ethoxy unit.

Synthesis of fluorene-RGD conjugate (2). Fluorene **1** (38 mg, 0.017 mmol) was dissolved in 2 mL H_2O. After adjusting the pH to 5.0–5.5 with 0.1 N NaOH (aq), sodium *N*-hydroxysulfonosuccinimide (5 mg, 0.023 mmol) and 1-(3-dimethylaminopropyl)-3-ethylcarbodiimide hydrochloride (6 mg, 0.026 mmol) were added. After stirring at 4 °C for 30 min, the pH of the reaction mixture was adjusted to 9 with 0.1 N NaOH (aq) and c(RGDfK) (10 mg, 0.016 mmol), dissolved in 0.5 mL of 0.1 M Na_2HPO_4 solution (pH = 9), was added. The reaction was stirred at room temperature for 24 h. Water was removed under reduced pressure, providing yellow oil, which was redissolved in CH_2Cl_2, dried over $NaSO_4$, filtered, and concentrated. The oil was washed several times with ether, then dried to afford **2** (43 mg, 90%) as a yellow oil. ^{1}H NMR (500 MHz, *d*-DMSO) δ: 8.55 (d, J = 8 Hz, 2H), 8.09 (d, J = 8 Hz, 2H), 7.94 (d, J = 8 Hz, 2H), 7.67 (d, J = 8 Hz, 2H), 7.60 (s, 2H), 7.52-7.17 (m, 5H), 7.50 (t, J = 8 Hz, 3H), 7.38-7.09 (m, 15H), 4.47 (t, J = 10 Hz, 5H), 4.12 (t, J = 9.5 Hz, 5H), 3.84 -3.52 (m, 118 H), 3.36 (s, 6H), 3.31-3.10 (m, 10H), 2.83 (t, 15.5 Hz, 2H), 2.74 (bt, 1H), 2.53-2.42 (m,6H), 1.74 (s, 1H), 1.63 (t, 16 Hz, 3H), 1.24 (s, 3H).^{13}C NMR (125 MHz, $CDCl_3$) δ: 175.48, 171.27, 168.48, 162.88, 159.99, 159.81, 156.71, 152.10, 152.12, 149.33, 140.97, 140.55, 136.41, 136.12, 136.10, 129.89, 129.64, 126.14, 125.80, 122.68, 122.53, 121.58, 121.26, 120.81, 119.32, 110.13, 71.83, 71.67, 71.25, 70.84, 70.67, 70.55, 70.43, 70.18, 69.94, 69.54, 69.39, 69.03, 68.48, 58.98, 56.42, 55.81, 55.56, 55.30, 54.99, 54.73, 52.18, 45.95, 44.25, 43.59, 43.19, 42.77, 42.38, 36.96, 36.87, 36.37, 36.29, 36.20, 35.81, 35.63, 35.23, 34.96, 34.70, 34.40, 34.12, 30.50, 29.67, 28.55, 25.81, 25.67, 25.54, 16.49, 15.74, 15.59, 15.44, 15.29, 14.54. HRMS-ESI: High resolution MS shows a series of ions centered around m/z 2246 [$C_{78}H_{79}N_{11}O_{12}S_2(C_2H_4O)_{30}C_2H_6$+Na]$^+$ which are fragments related to the various ethoxylate oligomers that differ by $\Delta m/z$ 44, an ethoxy unit.

Cell culture and incubation. U87MG cells were cultured in DMEM, supplemented with 10% FBS, 1% penicillin, and 1% streptomycin, at 37 °C under a 5% CO_2 environment. MCF 7 cells were cultured in MEM, also supplemented with 10% FBS, 1% penicillin, and 1% streptomycin, at 37 °C under a 5% CO_2 environment. No. 1 round 12 mm coverslips were treated with poly-D-lysine to improve cell adhesion and washed (3×) with PBS buffer solution. The treated coverslips were placed in 24-well plates, and 60 000 cells/well were seeded and incubated at the same conditions as indicated above until 75–85% confluency was reached on the coverslips. From a 3.04×10^{-4} M stock solution of probe **2** in PBS (7.4), a series of 1, 10, and 50 μM solutions in culture media were used to incubate both cell lines for 1 and 1.5 h. The dye solutions were removed and the coverslipped cells were washed abundantly with PBS (4×).

Cell fixing and mounting. Cells were fixed with 3.7% paraformaldehyde solution in pH = 7.4 PBS buffer for 10 min. The fixing agent was removed and washed (2×) with PBS. To reduce autofluorescence, a fresh solution of $NaBH_4$ (1 mg mL^{-1})

in pH = 8 PBS buffer was used for treating the fixed cells (2×). The coverslipped cells were then washed with buffer PBS (2×) and mounted on microscope slides using Prolong Gold (Invitrogen) as mounting media.

Confocal one-photon fluorescence imaging. Conventional (one-photon) fluorescence microsocopy images were recorded on an Olympus DSU IX-81 confocal microscope equipped with a Hamamatsu EM-CCD C9100 digital camera. Fluorescent images of the fixed cells were taken using a custom made filter cube (Ex: 377/50; DM: 409; Em: 525/40) and a Texas Red filter cube (Ex: 562/40; DM: 593; Em: 624/40) for probe **2** and Lysotracker Red, respectively.

Two-photon fluorescence imaging. Two-photon fluorescence microscopy (2PFM) imaging was performed on a modified Olympus Fluoview FV300 laser scanning confocal microscopy system equipped with a tunable Coherent Mira Ti:sapphire laser (115 fs pulse width, 76 MHz repetition rate), pumped by a 10 W Coherent Verdi frequency doubled Nd:YAG laser. The laser was tuned to 700 nm, modelocked, and used as the two-photon excitation source. Two-photon induced fluorescence was collected by a 60× microscope objective (UPLANSAPO 60×, N.A. = 1.35 Olympus). A high transmittance (>95%) short-pass filter (cutoff 685 nm, Semrock) was placed in front of the PMT detector within the FV300 scanhead in order to filter out background radiation from the laser source (700 nm).

Linear photophysical characterization. The absorption, fluorescence, and excitation anisotropy spectra of **1** were investigated in spectroscopic grade chloroform, acetonitrile (ACN), polytetrahydrofuran (pTHF), glycerol, and distilled water at room temperature. The steady-state absorption spectra of **1** were measured with an Agilent 8453 UV-visible spectrophotometer in 0.1, 1, and 10 mm path length quartz cuvettes with dye concentrations, C, 10^{-5} M $\leq C \leq 2 \times 10^{-3}$ M. The steady-state fluorescence and excitation anisotropy spectra were obtained with a PTI QuantaMaster spectrofluorimeter in 10 mm spectrofluorometric quartz cuvettes with C ~10^{-6} M. The fluorescence spectra were corrected for the spectral responsivity of the PTI emission monochromator and PMT. Excitation anisotropy measurements were performed in viscous pTHF and glycerol at room temperature and an "L-format" configuration was used. In viscous solvents, the influence of rotational depolarization processes are negligible during nanosecond fluorescence lifetimes, and excitation anisotropy reaches its fundamental value:[29]

$$r_0 = (3\cos^2\alpha - 1)/5 \quad (1)$$

where α is the angle between absorption $S_0 \rightarrow S_1$ and emission $S_1 \rightarrow S_0$ transition dipoles (S_0 and S_1 are the ground and first excited electronic state, respectively). Fluorescence lifetimes of **1**, τ, were obtained with a single photon counting system PicoHarp 300 under 76 MHz femtosecond excitation (MIRA 900, Coherent) with time resolution of ≈ 80 ps. The excitation laser beam was linearly polarized and oriented by the magic angle. Fluorescence quantum yields, Φ, of **1** were measured by a standard method relative to 9,10-diphenylanthracene in cyclohexane.[29] The intensity of linear light scattering I was measured in a 10 mm spectrofluorometric cuvette in the transverse direction to the excitation laser beam with corresponding intensity I_0. The femtosecond laser MIRA 900 (Coherent) was also used for these measurements. The dependencies of I on excitation wavelength λ and I_0 facilitated estimation of the nature of scattering mechanism and size of scattering centers.

2PA measurements. The 2PA spectra of **1** were determined by a standard two-photon induced fluorescence (2PF) method, relative to Rhodamine B in methanol.[18] A femtosecond laser Clark-MXR CPA-2010, with pulse duration ≈140 fs (FWHM), pumped an optical parametric generator/amplifier (TOPAS, Light Conversion) with a tuning range of 580–940 nm, pulse energies ≤0.15 μJ, and repetition rate 1 kHz, were used for excitation. The intensity of the 2PF was measured with a PTI QuantaMaster spectrofluorimeter in 10 mm quartz cuvettes with dye concentrations ~$(1–2) \times 10^{-5}$ M. The quadratic dependence of 2PF on average excitation power was verified for each excitation wavelength. The values of 2PA cross sections, δ_{2PA}, in the 720–900 nm spectral range were determined independently by the open aperture Z-scan method[46] using 76 MHz femtosecond excitation (MIRA 900, Coherent). The main characteristics of the MHz Z-scan methodology were described in ref. 47–49. A space filter with a 100 μm pinhole, electronic shutter VMM-T1 (Uniblitz) with 5 ms exposure time (less than 0.1 ms time to open), and neutral density filters were used in the experimental setup in order to avoid thermooptical distortion and accumulative effects of triplet population.

Conclusions

Water-soluble fluorene derivative **1** was synthesized in a straightforward manner. The steady-state absorption spectra were independent of solvent polarity while pronounced aggregation of **1** was observed in an aqueous medium, indicative of dimer formation, as suggested by light scattering measurements. Excitation anisotropy spectra of **1** in aprotic solvents provided valuable information on the spectral position and mutual orientation of ground to excited states transition dipoles, and disclosed excited electronic states participating in two-photon transitions. The fluorescence spectra of **1** were independent of excitation wavelength in aprotic solvents and exhibited weak solvatochromic effects. A high fluorescence quantum yield ~1.0 and a single exponential decay of the fluorescence emission was observed. In contrast, the fluorescence spectra of **1** in water exhibited an excitation wavelength dependence and double exponential decay in emission, indicative of specific solute–solvent effects.

The values of the 2PA cross sections increased monotonically in the short wavelength range (two-photon allowed transition) up to 3000–6000 GM. In the main 1PA band (formally two-photon forbidden), the efficiency of 2PA remained sufficiently high for practical applications (δ_{2PA} ~ 100–1000 GM) with commercially available femtosecond lasers. The increased values of δ_{2PA} in water, relative to the corresponding values in aprotic solvents, can be explained by possible cooperative electronic effects in molecular aggregates of **1**.

The corresponding RGDfK conjugate **2** clearly demonstrated the integrin-targeting ability of this new probe through 2PFM imaging of U87MG cells, providing a valuable new tool for the study of integrin-mediated processes in cells.

Acknowledgements

We wish to acknowledge the National Institutes of Health (1 R15 EB008858-01), the U.S. Civilian Research and Development Foundation (UKB2-2923-KV-07), the Ministry of Education and Science of Ukraine (grant M/49-2008), and the National Science Foundation (CHE-0832622) for support of this work.

Notes and references

1 W. Denk, J. H. Strickler and W. W. Webb, *Science*, 1990, **248**, 73.
2 J. D. Bhawalkar, A. Shih, S. J. Pan, W. S. Liou, J. Swiatkiewicz, B. A. Reinhardt, P. N. Prasad and P. C. Cheng, *Bioimaging*, 1996, **4**, 168.
3 W. R. Zipfel, R. M. Williams and W. W. Webb, *Nat. Biotechnol.*, 2003, **21**, 1369.
4 K. J. Schafer-Hales, K. D. Belfield, S. Yao, P. K. frederiksen, J. M. Hales and P. E. Kolattukudy, *J. Biomed. Opt.*, 2005, **10**, 051402–1.
5 M.-H. Ha-Thi, M. Penhoat, D. Drouin, M. Blanchard-Desce, V. Michelet and I. Leray, *Chem.–Eur. J.*, 2008, **14**, 5941.
6 H. Maeda, D. L. Tierney, P. S. Mariano, M. Banerjee, D. W. Cho and U. C. Yoon, *Tetrahedron*, 2008, **64**, 5268.
7 M. Zhang, M. Yu, F. Li, M. Zhu, M. Li, Y. Gao, L. Li, Z. Liu, J. Zhang, D. Zhang, T. Yi and C. Huang, *J. Am. Chem. Soc.*, 2007, **129**, 10322.
8 K. D. Belfield, M. V. Bondar, C. O. Yanez, F. E. Hernandez and O. V. Przhonska, *J. Mater. Chem.*, 2009, **19**, 7498.
9 G. S. He, R. Helgeson, T.-C. Lin, Q. Zheng, F. Wudl and P. N. Prasad, *IEEE J. Quantum Electron.*, 2003, **39**, 1003.
10 M. Akiba, A. Dvornikov and P. M. Rentzepis, *Proc. SPIE-Int. Soc. Opt. Eng.*, 2006, **6331**, 63310F.
11 C. C. Corredor, Z.-L. Huang, K. D. Belfield, A. R. Morales and M. V. Bondar, *Chem. Mater.*, 2007, **19**, 5165.
12 C. O. Yanez, C. D. Andrade, S. Yao, G. Luchita, M. V. Bondar and K. D. Belfield, *ACS Appl. Mater. Interfaces*, 2009, **1**, 2219.
13 D. W. Piston, *Trends Cell Biol.*, 1999, **9**, 66.
14 K. Konig, *J. Microsc.*, 2000, **200**, 83.
15 R. M. Williams, W. R. Zipfel and W. W. Webb, *Curr. Opin. Chem. Biol.*, 2001, **5**, 603.
16 A. Hayek, F. Bolze, J.-F. Nicoud, P. L. Baldeck and Y. Mely, *Photochem. Photobiol. Sci.*, 2006, **5**, 102.
17 T. R. Krishna, M. Parent, M. H. Werts, L. Moreaux, S. Gmouh, S. Charpak, A. M. Caminade, J. P. Majoral and M. Blanchard-Desce, *Angew. Chem., Int. Ed.*, 2006, **45**, 4645.
18 C. Xu and W. W. Webb, *J. Opt. Soc. Am. B*, 1996, **13**, 481.
19 P. Kaatz and D. P. Shelton, *J. Opt. Soc. Am. B*, 1999, **16**, 998.
20 W. J. Yang, M. S. Seo, X. Q. Wang, S.-J. Jeon and B. R. Cho, *J. Fluoresc.*, 2008, **18**, 403.
21 A. R. Morales, K. J. Schafer-Hales, A. I. Marcus and K. D. Belfield, *Bioconjugate Chem.*, 2008, **19**, 2559.
22 H. Y. Woo, D. Korystov, A. Mikhailovsky, T.-Q. Nguyen and G. C. Bazan, *J. Am. Chem. Soc.*, 2005, **127**, 13794.
23 A. Hayek, S. Ercelen, X. Zhang, F. Bolze, J.-F. Nicoud, E. Schaub, P. L. Baldeck and Y. Mely, *Bioconjugate Chem.*, 2007, **18**, 844.
24 A. Hayek, F. Bolze, J.-F. Nicoud, A. Duperray, A. Grichine, P. L. Baldeck and J.-C. Vial, *Nonlinear Opt., Quantum Opt.*, 2006, **35**, 155.
25 C. Lottner, K. C. Bart, G. Bernhardt and H. Brunner, *J. Med. Chem.*, 2002, **45**, 2079.
26 A. R. Morales, K. J. Schafer-Hales, C. O. Yanez, M. V. Bondar, O. V. Przhonska, A. I. Marcus and K. D. Belfield, *ChemPhysChem*, 2009, **10**, 2073.
27 J.-P. Leblanc, K. Rorrer and H. W. Gibson, *J. Org. Chem.*, 1994, **59**, 674.
28 K. D. Belfield, M. V. Bondar, F. E. Hernandez, O. V. Przhonska and S. Yao, *Chem. Phys.*, 2006, **320**, 118.
29 P. Schouwink, H. V. Berlepsch, L. Dahne and R. F. Mahrt, *Chem. Phys.*, 2002, **285**, 113.
30 C. F. Bohren, D. Huffman, *Absorption and Scattering of Light by Small Particles*, John Wiley, New York, 1983.
31 J. R. Lakowicz, *Principles of Fluorescence Spectroscopy*, Kluwer, New York, 2nd edn, 1999.
32 X.-Q. Zhu, M.-T. Zhang, A. Yu, C.-H. Wang and J.-P. Cheng, *J. Am. Chem. Soc.*, 2008, **130**, 2501.
33 O. Bismuth, N. Friedman, M. Sheves and S. Ruhman, *Chem. Phys.*, 2007, **341**, 267.
34 W. L. Peticolas, *Annu. Rev. Phys. Chem.*, 1967, **18**, 233.
35 K. D. Belfield, M. V. Bondar, F. E. Hernandez, O. V. Przhonska and S. Yao, *J. Phys. Chem. B*, 2007, **111**, 12723.
36 J. M. Hales, D. J. Hagan, E. W. Van Stryland, K. J. Schafer, A. R. Morales, K. D. Belfield, P. Pacher, O. Kwon, E. Zojer and J. L. Bredas, *J. Chem. Phys.*, 2004, **121**, 3152.
37 K. D. Belfield, M. V. Bondar, F. E. Hernandez, O. V. Przhonska and S. Yao, *Chem. Phys.*, 2006, **320**, 118.
38 E. Collini, C. Ferrante and R. Bozio, *J. Phys. Chem. B*, 2005, **109**, 2.
39 E. Ruoslahti and M. D. Pierschbacher, *Science*, 1987, **238**, 491.
40 J. D. Hood and D. A. Cheresh, *Nat. Rev. Cancer*, 2002, **2**, 91.
41 W. Cai and X. Chen, *Nat. Protoc.*, 2008, **3**, 89.
42 A. E. Aplin, A. K. Howe and R. L. Juliano, *Curr. Opin. Cell Biol.*, 1999, **11**, 737.
43 S. K. Sastry and K. Burridge, *Exp. Cell Res.*, 2000, **261**, 25.
44 G. Shtengel, J. A. Galbraith, C. G. Galbraith, J. Lippincott-Schwartz, J. M. Gillette, S. Manley, R. Sougrat, C. M. Waterman, P. Kanchanawong, M. W. Davidson, R. D. Fetter and H. F. Hess, *Proc. Natl. Acad. Sci. U. S. A.*, 2009, **106**, 3125.
45 A. R. Morales, C. O. Yanez, K. J. Schafer-Hales, A. I. Marcus and K. D. Belfield, *Bioconjugate Chem.*, 2009, **20**, 1992.
46 M. Sheik-Bahae, A. A. Said, T. H. Wei, D. J. Hagan and E. W. Van Stryland, *IEEE J. Quantum Electron.*, 1990, **26**, 760.
47 M. Falconieri and G. Salvetti, *Appl. Phys. B: Lasers Opt.*, 1999, **69**, 133.
48 A. Gnoli, L. Razzari and M. Righini, *Opt. Express*, 2005, **13**, 7976.
49 A. Nag, A. Kr. De and D. Goswami, *J. Phys. Conf. Ser.*, 2007, **80**, 012034.

